Ecological Indicators 101 (2019) 954–962

Contents lists available at ScienceDirect

Ecological Indicators

journal homepage: www.elsevier.com/locate/ecolind

Original Articles

Effects of nitrogen deposition on water use efficiency of global terrestrial ecosystems simulated using the IBIS model

Xuehe Lu[a,b], Weimin Ju[b,*], Hong Jiang[b,*], Xiuying Zhang[a], Jinxun Liu[c], Jason Sherba[c], Songhan Wang[a,b]

[a] Jiangsu Provincial Key Laboratory of Geographic Information Science and Technology, Xianlin Avenue 163, Nanjing 210093, China
[b] International Institute for Earth System Science, Nanjing University, Xianlin Avenue 163, Nanjing 210093, China
[c] USGS Western Geographic Science Center, Menlo Park, CA 94025, USA

ARTICLE INFO

Keywords:
Water use efficiency
Nitrogen deposition
Model simulation
Climate change
Carbon and nitrogen coupling

ABSTRACT

Nitrogen (N) deposition changes the availability of N in ecosystems and regulates carbon and water cycles, including ecosystem water use efficiency (WUE). In recent decades, N deposition has been increasing rapidly, especially at several hotspots in China, Europe and the U.S. In this study, a process-based terrestrial ecosystem model, IBIS (Integrated BIosphere Simulator), was used to simulate the effects of N deposition on WUE globally. The results indicated that increasing N deposition led to a global increase in WUE of 0.005 g C kg^{-1} H_2O on average over the first 10 years of the 21st century. The effects of N deposition on WUE were more evident in certain hotspots than in other parts of the world. The effect of N deposition on gross primary productivity (GPP) determined the change in WUE. In particular, high N deposition led to decreased ET and consequently increased the WUE in southeastern China. Moreover, increased N deposition has significantly enhanced the WUE in response to elevated CO_2 in southeastern China, indicating the importance of N deposition in regulating the terrestrial carbon cycle.

1. Introduction

During leaf photosynthesis, stomata open to absorb CO_2, which leads to loss of water vapour from leaves (Berry et al., 2010). The trade-off between carbon gain and water loss in terrestrial ecosystems can be measured as the water use efficiency (WUE) of the ecosystem, which is the ratio of annual gross primary productivity and annual evapotranspiration (ET) (Huang et al., 2015; Ito and Inatomi, 2012; Knauer and Zaehle, 2017; Liu et al., 2015). The WUE is a key parameter for understanding the metabolism of carbon and water-based economics of terrestrial ecosystems (Keenan et al., 2013). An in-depth study of WUE will provide insights into variations of the carbon and water cycles under climate change and improve our ability to predict the feedbacks of ecosystems to climate in the future.

The carbon and water cycles of terrestrial ecosystems are both regulated by the amount of available nitrogen (N) in the soil. However, atmospheric N deposition has altered the available N content (Niu et al., 2016) due to the rapid increase of N deposition in the past few decades (Galloway et al., 2004). Studies have indicated that N deposition on land has increased to 59–68 Tg N yr^{-1} (Vet et al., 2014) and may increase in the future (Lamarque et al., 2013).

N deposition impacts WUE from both functional and structural aspects. The function of carbon assimilation in terrestrial ecosystems is enhanced by the increase of N deposition (Fernández-Martínez et al., 2014). Studies have indicated that N deposition has led to an increase of 0.41 Pg C yr^{-1} in the net primary productivity (NPP) of global forests (Du and Vries, 2018) and an increase of 0.27 ± 0.13 Pg C yr^{-1} in the total net carbon sink using a stoichiometric approach (Wang et al., 2017). Stomatal conductance might be reduced by increases in N deposition (Cramer et al., 2009; Köhler et al., 2012; Livingston et al., 1999), which may cause a decrease in transpiration. Furthermore, changes in ecosystem structure cause diverse changes in ET when upscaling from the leaf to the ecosystem level (Huang et al., 2015). For instance, an enhanced leaf area index (LAI) results in an increase of canopy transpiration and interception. However, the increase in LAI might lead to a decline in soil evaporation when less solar radiation penetrates the canopy to the soil surface (Hungate et al., 2002). N deposition increases carbon allocation in leaves (Litton et al., 2007) and makes LAI increase. For example, in southeastern China the trend of LAI attributed to N deposition is generally larger than 0.0050 yr^{-1} (Piao

* Corresponding authors.
E-mail addresses: luxh@nju.edu.cn (X. Lu), juweimin@nju.edu.cn (W. Ju), jianghong@nju.edu.cn (H. Jiang), jxliu@usgs.gov (J. Liu), jsherba@usgs.gov (J. Sherba).

https://doi.org/10.1016/j.ecolind.2019.02.014
Received 29 September 2018; Received in revised form 25 January 2019; Accepted 8 February 2019
Available online 13 February 2019
1470-160X/ © 2019 Elsevier Ltd. All rights reserved.

et al., 2015). Therefore, the effect of N deposition on the structure of the ecosystem leads to changes in ET.

CO_2 and N deposition are major factors associated with global change and have an important impact on WUE. Multi-model assessments have indicated that changes in WUE in recent decades attributed to N deposition were 26 ± 3% on average (Zhou et al., 2017), which is much less than that attributed to CO_2 fertilization effects (Huang et al., 2015). Due to the theory of progressing N limitation under elevated CO_2 (Luo et al., 2004), N deposition should have a greater ability to change the ecosystem WUE. However, the increase in N deposition is mainly concentrated in areas with strong human activities (Vet et al., 2014) and the N demand of different ecosystems is not equivalent (Koven et al., 2015; Yu et al., 2014). Therefore, the average impact of N deposition on global WUE is not evident. The current research has confirmed that the significantly enhanced N deposition observed in certain regions increases the productivity of the ecosystem (Fernández-Martínez et al., 2014; Yu et al., 2014), changed the water cycle processes (Lu et al., 2018), and caused changes in structural parameters, such as the LAI (Zhu et al., 2016). However, in-depth studies on the effects of N deposition on the temporal and spatial dynamics of WUE in N deposition hotspots have not been performed. In addition, under elevated CO_2, the coupling effects of N deposition and CO_2 fertilization on WUE in N deposition hotspots are still unclear.

Therefore, this study investigates the roles of N deposition in driving the changes of global WUE under elevated CO_2 in different regions of the globe. The process-based ecosystem model forced by spatially and temporally variant N deposition and climate data is implemented to (1) isolate the contribution of N deposition to WUE changes in different regions of the globe; (2) attribute the changes of WUE to changes in ecosystem function and structure caused by N deposition; (3) assess the integrated effects of elevated CO_2 and N deposition on WUE at global and regional scales.

2. Materials and methods

2.1. Definition of ecosystem WUE

Following previous studies (Beer et al., 2009; Huang et al., 2015; Zhu et al., 2011), the ecosystem annual mean WUE is defined as follows:

$$\mathrm{WUE} = \frac{\mathrm{GPP}}{\mathrm{ET}} \tag{1}$$

where GPP is the annual ecosystem gross primary productivity ($\mathrm{g\,m^{-2}\,yr^{-1}}$) and ET is annual evapotranspiration (mm). In this study, both GPP and ET were simulated using the IBIS model at a spatial resolution of 0.5 × 0.5°.

Grids with Normalized Difference Vegetation Index (NDVI) values below 0.1 were excluded in the calculation of globally and regionally averaged WUE. The NDVI datasets used in this study is the third generation NDVI from Advanced Very High Resolution Radiometer sensors (AVHRR NDVI3g) (Pinzon and Tucker, 2014).

2.2. Model description

The IBIS model is a process-based global vegetation dynamic model developed by Foley et al. (1996). To better simulate the coupling between carbon (C) and N cycles, Liu et al. (2005) modified this model, and the modified version of IBIS (IBIS-CN) (Liu et al., 2005) was used here. This model is able to simulate the controls of N availability on both aboveground C assimilation and soil organic carbon (SOC) decomposition and capture the feedback of C assimilation on N availability.

In the IBIS-CN model, vegetation photosynthesis and stomatal conductance (Gs) are simulated using the Farquhar equation (Farquhar et al., 1980) and the Ball-Berry model (Ball et al., 1987), respectively. In the Farquhar equation, the leaf maximum carboxylation rate is downscaled by the leaf available N:

$$V_m = (B_{Vmax}/B_L) \times V_{max} \tag{2}$$

where V_m is the actual leaf maximum carboxylation rate, B_{Vmax} is the optimal C:N ratio for foliage at which the leaf maximum carboxylation rate (V_{max}) occurs, and B_L is the actual foliar C:N ratio, and it is determined by a C:N modifierK_{CN}.

K_{CN} is quantified as follows (Liu et al., 2005):

$$\begin{aligned} K_{CN} &= (N_M - 2N_{Mmin})/(N_{Mmax} - 2N_{Mmin}) \\ dN_M &= N_D + N_{FX} + N_{MI} - N_{IM} - N_{LH} - N_{UP} - N_{VL} \end{aligned} \tag{3}$$

where N_{Mmin} and N_{Mmax} are the minimum and maximum soil available N thresholds for N control calculation, respectively; N_M is the total available N in the soil for plant growing and updated every time step by net daily change rate (dN_M); N_D is the atmospheric N deposition, N_{FX} is the plant N fixation; N_{MI} and N_{IM} are the mineralized N and immobilized N, respectively; N_{LH} is the soil N leaching, N_{UP} is the plant N uptake, and N_{VL} is the soil volatile N.

Daily N uptake (N_{UP}) is determined according to N demand and N storage (N_{ST}) and calculated as follows:

$$N_{UP} = \begin{cases} \mathrm{NPP_b}/B_A - N_{ST}, & N_{ST} \leqslant 0.5\mathrm{NPP_b}/B_A \quad (a) \\ 0.5\mathrm{NPP_b}/B_A, & N_{ST} > 0.5\mathrm{NPP_b}/B_A \quad (b) \end{cases} \tag{4}$$

where B_A is the C:N ratio of the daily biomass net primary productivity ($\mathrm{NPP_b}$) and $\mathrm{NPP_b}/B_A$ is the N demand for plant for biomass construction.

The foliar C:N ratio B_L is described as follows:

$$B_L = B_{Lmax} - K_{CN}(B_{Lmax} - B_{Lmin}) \tag{5}$$

where B_{Lmax} and B_{Lmin} are the prescribed maximum and minimum foliage C:N ratios, respectively.

The LAI affects the WUE due to its effects on both GPP and ET. In the IBIS-CN model, LAI is simulated according to foliage biomass and the specific leaf area. The former is updated on the basis of the amount of fixed C and the allocation ratio to leaves, which changes with the modifier K_p:

$$\begin{aligned} A_R &= A_{Rmax} - K_p(A_{Rmax} - A_{Rmin}) \\ A_L &= A_{LR} - A_R \\ A_W &= 1 - A_{LR} \end{aligned} \tag{6}$$

where A_R, A_L and A_W represent the ratios of fixed C allocated to the root, leaf and wood components, respectively; A_{Rmax} and A_{Rmin} are the prescribed maximum and minimum ratios of C allocated to the roots, respectively; A_{LR} is the prescribed ratio of C allocated to the roots and leaves; and K_p is the modifier, which is determined by the total soil N availability. K_p is quantified as follows:

$$K_p = \begin{cases} [(N_M - 0.2)/(N_{Mmax} - N_M)]^{0.5} & (N_M < N_{Mmax}) \\ 1 & (N_M \geqslant N_{Mmax}) \end{cases} \tag{7}$$

where N_M and N_{Mmax} are the total soil N and maximum N available in the soil, respectively.

The controls on N deposition in ecosystem WUE are shown in Fig. 1, and details about the parameters are listed in Table S1. The leaf maximum carboxylation rate (V_m) affects the photosynthesis rate and is adjusted by leaf C:N (B_L), which is determined by the total soil N availability (N_M) through the adjustment factor K_{CN} (Eq. (5)). The photosynthesis rate and stomatal conductance (G_s) are linearly linked (Ball et al., 1987). Therefore, soil available N affects G_s and consequently leaf transpiration (Tr_L). In addition, N_M determines the allocation of C fixed through photosynthesis into different biomass C pools. With the increase of N_M, more C will be allocated to leaves. As a consequence, LAI will increase. LAI is an important determinant of canopy GPP (GPP_E), and it also significantly affects evapotranspiration of ecosystem (ET_E) via its roles in canopy transpiration and evaporation

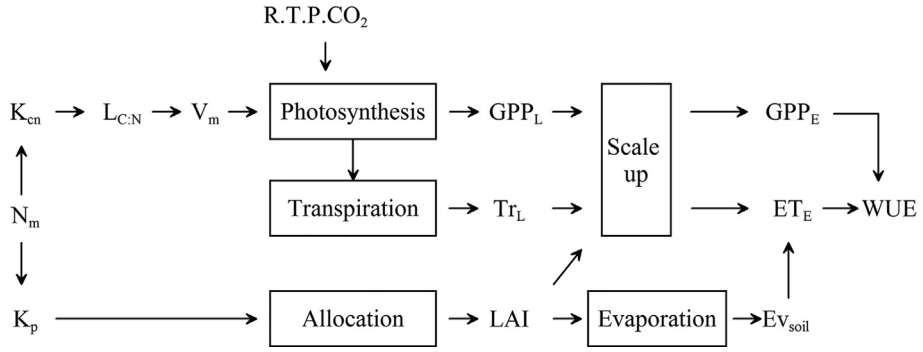

Fig. 1. Nitrogen controls on WUE in the IBIS model.

from water intercepted by the canopy and from soils. Accordingly, the IBIS-CN model properly describes the effects of soil N availability on the C and water cycles via N mineralization, deposition, uptake by plants and other variables of N fluxes (Eq. (3)). Thus, the effects of N deposition on the WUE at the global scale can be modelled.

IBIS has been validated at regional and global scales in previous studies (Cramer et al., 2001; Kucharik et al., 2000; Lu et al., 2016a; Zhang et al., 2013; Zhu et al., 2012). Recently, Lu et al. used data from 37 N addition experiments (Lu et al., 2016a) and confirmed that IBIS-CN was able to properly simulate the ability of N deposition to enhance the above-ground NPP.

2.3. Model simulations

Three different simulations were conducted to evaluate the effects of N deposition on the global WUE. The details on these simulations are listed in Table 1. In scenario 1 (S1), all of the driving factors were dynamic. In scenarios 2 (S2) and 3 (S3), the N deposition and CO_2 concentrations were kept at values observed in 1970, respectively. The difference in WUE between S1 and S2 was used to quantify the effect of N deposition on WUE. Similarly, the effect of CO_2 fertilization on WUE was the difference between S1 and S3.

Before performing three different simulations, the average values of temperature, precipitation, CO_2 concentration, and N deposition rates during the period 1901–1959 were used in conjunction with other model initial datasets to spin up the IBIS model until the C and N pools reached equilibrium. Then, the model was run from 1960 to 2009 with different scenarios of temperature, precipitation, CO_2 and N deposition (Table 1). Monthly temperature and precipitation data were collected from the CRU (Climatic Research Unit) dataset. The global atmospheric CO_2 concentration was retrieved from Earth System Research Laboratory (ESRL) measurements recorded by the National Oceanic and Atmospheric Administration (NOAA).

Monthly N deposition during 1970 and 2009 was estimated using satellite NO_2 column density data and the atmosphere chemistry transfer model MOZART (Model for Ozone and Related Chemical Tracers) (Lu et al., 2016b). The spatial distribution of global N deposition is not homogeneous. In some regions, such as China, India, Europe and the USA, N deposition changed significantly (Galloway et al., 2008; Lu et al., 2016b) and presented rates above ± 0.3 $g\,N\,m^{-2}\,yr^{-1}$ over the past 40 years.

2.4. Model validation

2.4.1. Validation with site observations

To validate the ability of the IBIS to simulate annual WUE, we collected WUE values derived from flux tower measurements in previous studies (Beer et al., 2009; Keenan et al., 2013; Tang et al., 2014). A total of 37 sites satisfying the following criteria were selected: (1) data were available more than 3 years; (2) the site was located within the extent of the IBIS simulation; and (3) the ecosystem type was typically natural. The site details are listed in Table S2, and the distribution is shown in Fig. 2b.

Fig. 2a presents a comparison of the simulated WUE and the tower-based WUE at 37 sites. The R^2 and average absolute error of the simulated WUE against the tower-based WUE are 0.73 and 11.3%, respectively. However, the IBIS-CN model tended to slightly overestimate low WUE conditions or underestimate high WUE conditions. The R^2 of the simulated WUE versus the tower-based WUE for different types of ecosystems ranged from 0.6 (DBF) to 0.81 (grassland). The discrepancy between the simulated and tower-based WUE might be attributed to the following reasons. First, the model grids were $0.5 \times 0.5^{\circ}$, which is much larger than the footprints of the towers. The vegetation, climate, and soil conditions of the $0.5 \times 0.5^{\circ}$ grids were not identical to the conditions at the tower sites. Second, the IBIS model was run at hourly steps with meteorological data generated from monthly CRU climate data, which might differ from tower observations. Third, the IBIS-CN model was parameterized on the basis of plant functional types. In reality, considerable changes in parameters are observed, even for a specific plant function type. The abovementioned and other deficiencies might induce uncertainties in the simulated WUE and should be kept in mind. Nevertheless, the validation indicated the ability of the IBIS-CN to capture WUE variations among different plant function types and different sites, and it is applicable to simulate global WUE.

2.4.2. Validation of the simulated global mean WUE

To further validate the IBIS-CN model, the simulated global mean WUEs were compared with the values reported in previous studies based on model simulations and remote sensing (Table 2). The global mean WUE simulated by the IBIS-CN model was 1.72 $g\,C\,kg^{-1}$ H_2O

Table 1
Design of the simulation experiments.

Experiment	Time range	Details of driving factors				
		Temperature	Precipitation	CO_2	N deposition	Description
Spin up	1910–1959	Using model initial datasets				
S1	1960–2009	Change	Change	Change	Change	All factors change
S2	1960–2009	Change	Change	Change	1970	No change in nitrogen
S3	1960–2009	Change	Change	1970	Change	No change in CO_2

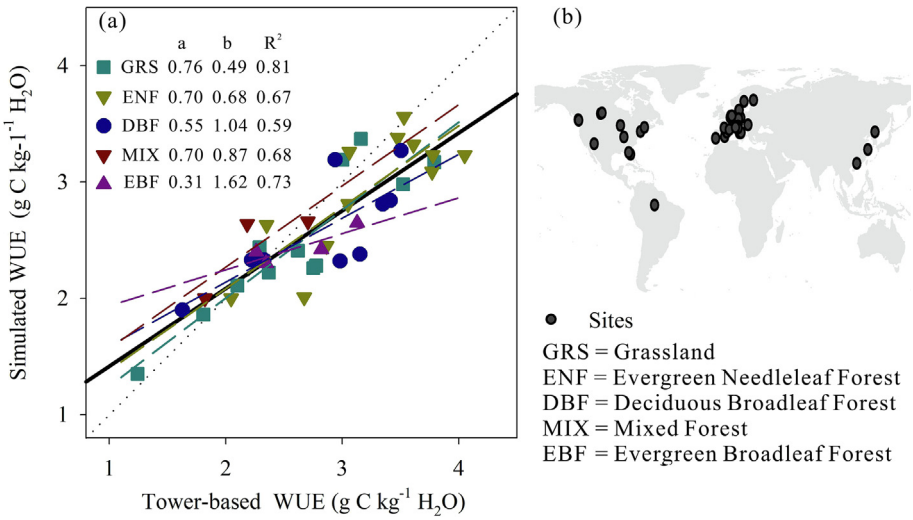

Fig. 2. Annual average WUE simulated using the IBIS-CN compared with tower-based WUE (a) at 37 FLUXNET sites (b).

during 2000–2009, and this value was almost identical to the global mean WUE of 1.71 g C kg^{-1} H_2O retrieved from MODerate resolution Imaging Spectroradiometer (MODIS) products during 2000–2013 (Tang et al., 2014). The global mean WUE simulated by the IBIS-CN was close to the WUE from the Model Tree Ensembles (MTE) and the WUE simulated by C-N coupling models (Sun et al., 2016). In addition, our simulated global mean WUE was within the range of 2.14 ± 0.6 g C kg^{-1} H_2O reported in a literature review by Jasechko et al. (2013). However, the global mean WUE simulated by the IBIS-CN was lower than the global mean WUE of 2.0 ± 0.3 g C kg^{-1} H_2O simulated by 4 process-based models (including two C-N coupling models) (Sun et al., 2016).

2.5. Response of WUE to CO_2 elevation

The WUE response to CO_2 elevation from 1970 to 2009 was assessed as follows:

$$R_{i+1} = \frac{WUE_{i+1} - WUE_i}{CO_{2i+1} - CO_{2i}} \quad (8)$$

where R represents the change in WUE associated with CO_2 elevation (g C kg^{-1} H_2O ppm^{-1}), WUE is the water use efficiency (g C kg^{-1} H_2O), CO_2 is the atmospheric CO_2 concentration (ppm), and subscripts i and i + 1 represent years from 1970 to 2009. The difference in R between S1 and S2 indicates the effects of N deposition on the WUE response to elevated CO_2.

3. Results

3.1. Spatial patterns of simulated WUE

Fig. 3 shows the spatial distribution of the simulated annual WUE averaged over the period from 2000 to 2009. The areas with high WUE (above 3.0 g C kg^{-1} H_2O) were mainly located in boreal forests in Northern Europe, Eastern Russia and Canada and maritime region of Eastern North America. The WUE was also high in western Europe, southeastern China, eastern North America, and areas dominated by tropical forests (close to 2.5 g C kg^{-1} H_2O). The WUE in central Asia, the Qinghai Tibet Plateau, India, and western North America was low and ranged from 0 to 1.0 g C kg^{-1} H_2O. The global mean annual WUE simulated by the IBIS-CN model was 1.72 g C kg^{-1} H_2O.

The effects of N deposition on WUE have increased along with increases in N deposition over the past 40 years (Fig. 4c). The period in which N deposition had the greatest effect on the WUE was the first 10 years of the 21st century. During this period, increasing N deposition led to an increase in the global mean WUE of 0.005 g C kg^{-1} H_2O (Fig. 4c). The areas in which N deposition had a large effect on WUE are mainly located in eastern China, the eastern United States, and central and northern Europe (Fig. 4a). In these regions, N deposition changed more than ± 0.3 g N m^{-2} yr^{-1} relative to the baseline values in 1970 (Fig. 4b).

N deposition changed evidently in eastern China, Europe, eastern USA and India which can be called N deposition hotspots. Changes in N deposition led to WUE increases of more than 0.06 g C kg^{-1} H_2O in eastern China, where N deposition generally increased by more than 0.9 g N m^{-2} yr^{-1} from 2000 to 2009 relative to the values in 1970 (Table 3). In Europe, decreases in N deposition in some areas led to a decline in WUE. In some parts of Germany and Russia, in which

Table 2
Validation of the IBIS-simulated global WUE.

ID	Method	Time range	WUE (g C kg^{-1} H_2O)	Reference	This study (g C kg^{-1} H_2O)
1	MODIS	2000–2013	1.71	(Tang et al., 2014)	1.72 (2000–2009)
	Flux tower		1.9		
2	Literature review	Multi-year average	2.14 ± 0.6	(Jasechko et al., 2013)	1.70 (1990–2009)
3	CABLE	1982–1986	1.67	(Huang et al., 2015)	1.62 (1982–1986)
		2004–2008	1.72		1.73 (2004–2008)
4	CLM4CN	1982–1986	1.93		1.62 (1982–1986)
		2004–2008	2.01		1.73 (2004–2008)
5	MTE	2000–2008	1.8 ± 0.6	(Sun et al., 2016)	1.72 (2000–2008)
	4 process-based models	2000–2009	2.0 ± 0.3		1.72 (2000–2009)

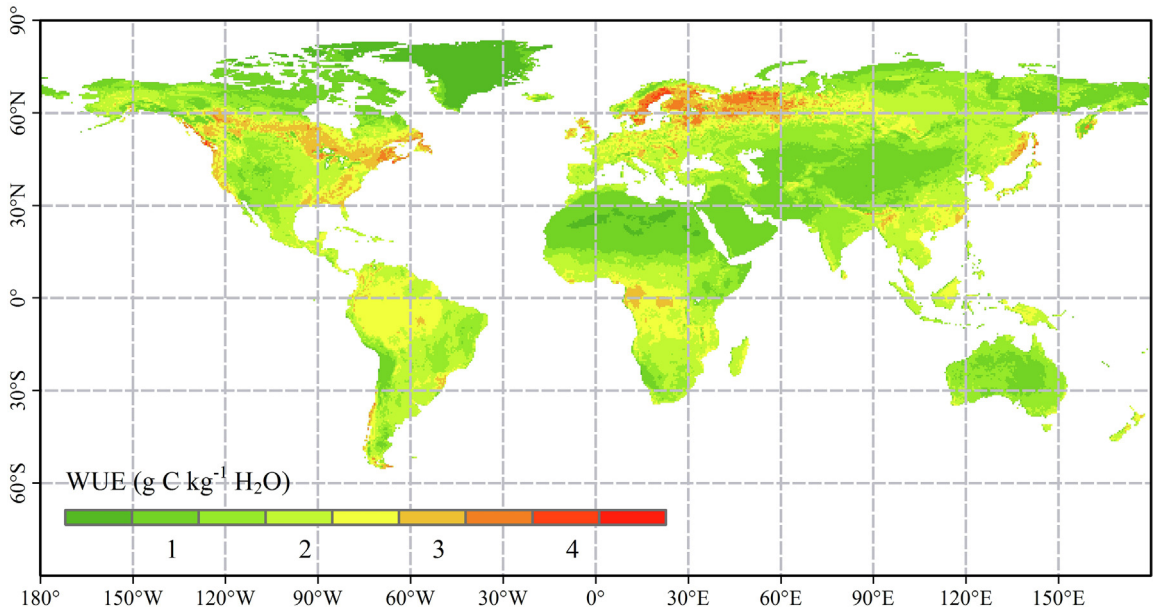

Fig. 3. Simulated annual mean WUE averaged over the period of 2000 to 2009.

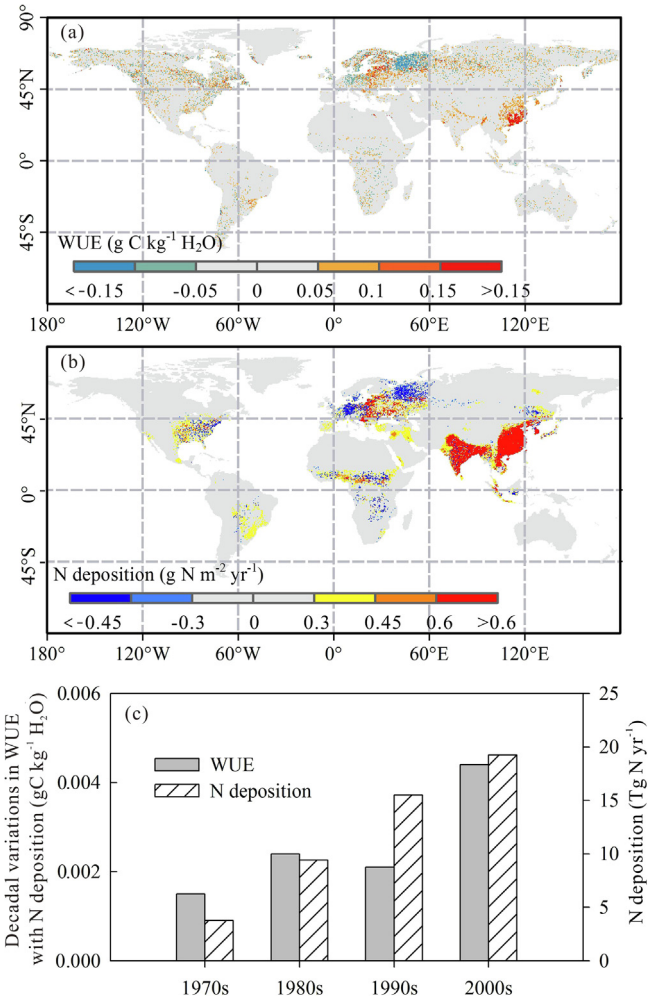

Fig. 4. Effects of N deposition on WUE. (a) Difference in WUE between the simulation with the N deposition change (S1) and no N deposition change (S2) in the 2000s; (b) spatial distribution of the difference in N deposition between S1 and S2 in the 2000s; and (c) decadal variations in WUE with N deposition (S1-S2).

temperate forests and boreal forests are widely distributed, decreases in N deposition induced a decline in WUE of 0.097 g C kg^{-1} H_2O on average. In contrast, increasing N deposition was observed in eastern Europe, which led to a rise in WUE of approximately 0.072 g C kg^{-1} H_2O. In total, changes in N deposition led to a decrease in WUE of 0.022 g C kg^{-1} H_2O over Europe from 2000 to 2009 (Table 3). In the eastern United States, areas showing increases and decreases in N deposition were staggered. Overall, N deposition increased slightly and caused a small increase in WUE of 0.006 g C kg^{-1} H_2O over the eastern United States (Table 3). Details on the changes in the WUE in N deposition hotspots are shown in Table 3.

3.2. Effects of N deposition on GPP and ET

WUE is determined by GPP and ET, which both were affected by N deposition. The spatial distribution of N deposition-induced changes in GPP is shown in Fig. 5a. N deposition increased significantly in subtropical forests in southeastern China, temperate forests in Europe, and temperate and subtropical forests in the eastern United States, with N deposition enhancing GPP by 4.89% (103 g m^{-2} yr^{-1}), 3.92% (44 g m^{-2} yr^{-1}) and 1.61% (36 g m^{-2} yr^{-1}) on average from 2000 to 2009 in these three regions, respectively. However, in certain western European temperate forests and Russian boreal forests, the decrease in N deposition (by 60.23% from 2000 to 2009 relative to the value in 1970) caused a decrease in GPP to approximately 3.87% (32 g m^{-2} yr^{-1}).

As shown in Fig. 5b, the simulated effects of N deposition on ET were complex. For certain temperate forests in Europe and the United States, increases in N deposition enhanced ET. However, the significant increase of N deposition induced a decrease in ET of 10.1 mm yr^{-1} in southeastern China. In Europe, a decrease in N deposition led to obvious declines in ET (Fig. 5b). Large changes in ET have been observed in certain tropical forests, in which the average change in N deposition was ± 0.2 g N m^{-2} yr^{-1}, and GPP changed marginally in these areas.

At the global scale, rising N deposition has led to a much greater increase in GPP (0.3%) than ET (0.05%). Therefore, the global WUE increase induced by N deposition was mainly driven by a larger enhancement of GPP over the past 40 years. The percentages of the changes in GPP and ET at N deposition hotspots are shown in Fig. 5c. The change of GPP was the dominant driver for the variation of WUE at all N deposition hotspots. The GPP of subtropical forests in southeastern

Table 3
Changes in N deposition and effects on WUE in Hotspots.

Hotspots	N deposition differences between the 2000s and 1970 (g m^{-2} yr^{-1})	Effect of changes in N deposition on the WUE of typical vegetation types (g C kg^{-1} H_2O)				
		Tropical forest	Temperate forest	Boreal forest	Grassland	Regional average
Eastern China	+0.93	+0.1149	+0.065	+0.034	+0.003	+0.061
Europe	−0.07		+0.006	−0.094	+0.006	−0.022
Eastern USA	+0.08	+0.019	+0.007		+0.005	+0.006

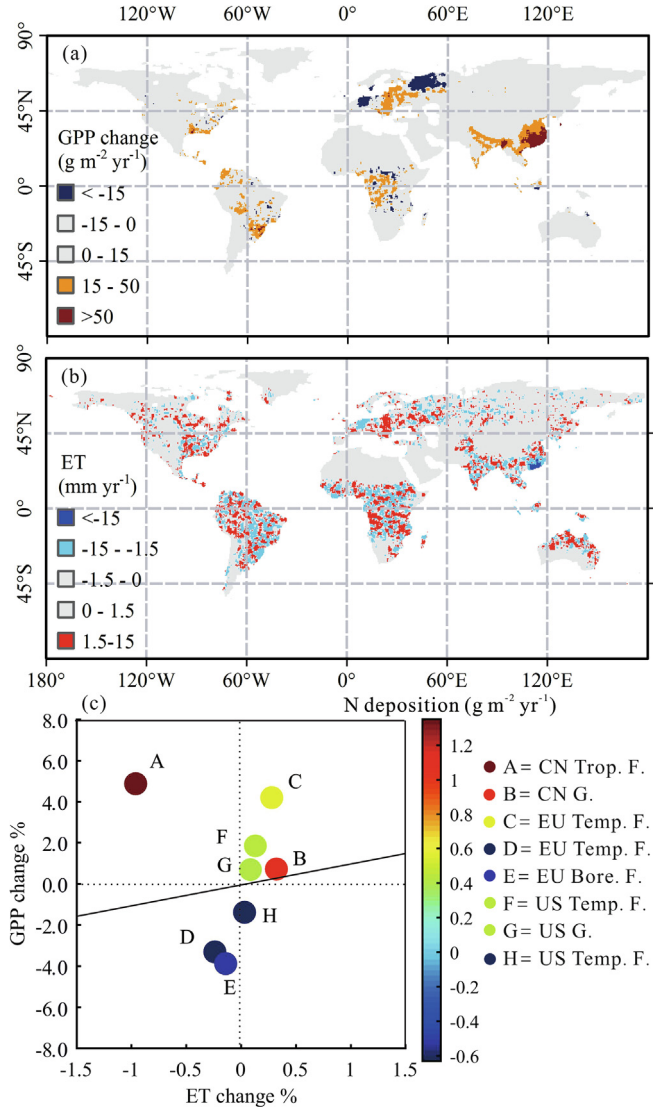

Fig. 5. Changes of GPP (a) and ET (b) from 2001 to 2009 relative to the values in 1970 over the globe induced by N deposition and (c) percentage of changes in GPP and ET at N deposition hotspots. In panels (a) and (b), the values reflect differences in GPP and AET between simulations S1 and S2. Positive values indicate that changes of N deposition enhanced GPP and ET and vice versa. In panel (c), the percentage change of GPP and ET represents the average differences between simulations S1 and S2 in N deposition hotspots. CN, EU and US are represented China, Europe and United States, respectively. Trop, Temp and Bore are represented tropical, temperate and boreal, respectively. F and G are represented forest and grassland, respectively.

China exhibited the greatest increase due to the highest increase of N deposition. However, in this region, increasing N deposition had a negative effect on ET, which was different from the change of ET with increasing N deposition at other hotspots. Consequently, rising N deposition induced the largest increase of WUE in southeastern China relative to other regions.

3.3. Coupling effects of elevated CO_2 and increased N deposition on WUE

Elevated CO_2 levels had a greater enhancing effect on WUE than N deposition (Fig. 6a). From 2000 to 2009, the global means of WUE were 1.71 and 1.58 g C kg^{-1} H_2O in simulations S2 (N deposition was temporally invariant with time) and S3 (CO_2 concentration was temporally invariant), respectively. Therefore, CO_2 elevation played a more important role in enhancing WUE than N deposition over the past 40 years. The WUE response to CO_2 concentration (R), which was calculated using Eq. (8) and outputs from simulation S1, was used to quantify the effect of CO_2 elevation on WUE. The response ratio (R) exhibited a downtrend in the past 40 years (Fig. 6b), implying that the effect of increased CO_2 on WUE declined over time.

Based on the differences of R between the results of simulations S1 and S2, increased N deposition promoted the effect of increased CO_2 on WUE. From 2000 to 2009 at the global level, N deposition led to an increase in R by 0.0001 g C kg^{-1} H_2O ppm^{-1} CO_2 on average (Fig. 6c). Strong effects of N deposition on R were found at N deposition hotspots. The positive effects of N deposition on R were more evident in subtropical forests of southeastern China and temperate forests of Europe. A T-test indicated that N deposition significantly affected the R values in the subtropical forests of southeastern China, where the highest global N deposition rate was observed. Therefore, the increase in N deposition significantly altered the coupling between carbon and water cycles in this region. In Europe, where temperate and boreal forests are widely distributed, N decreased in hotspots, with limited the effects on R. From a global perspective, increasing N deposition had a small impact on the WUE response to increasing CO_2. However, in areas with significant increases in N deposition, the large supply of N from atmospheric deposition enhanced the effect of increased CO_2 on WUE.

4. Discussion

4.1. Temporal and spatial changes of N deposition on WUE

According to the simulation results, increases in WUE under N deposition have been strengthened over the past 40 years. At the end of our simulation from 2000 to 2009, N deposition increased the WUE by 0.005 g C kg^{-1} H_2O on average. This result is similar to results observed by the CLM4CN simulation, which indicated that the average change trend of WUE from N deposition was 0.0004 g C kg^{-1} H_2O yr^{-1}, with a total of 0.004 g C kg^{-1} H_2O for 10 years (Huang et al., 2015). Comparisons of model results have shown that N deposition is an important factor that promotes global WUE, and its effect is second only to that of CO_2. Our results indicated that three main regions could account for the impact of N deposition on global WUE: southeast China, Europe and eastern USA. In all of these regions, N deposition changes over the past 40 years were significantly higher than that in other parts of the world (Lu et al., 2016b).

In addition, these hotspots were able to contribute more to the global WUE increase not only because of increases in N deposition but also because of the demand for ecosystem nitrogen. Ecosystems are constrained by a variety of nutrients, such as carbon, nitrogen and phosphorus. Carbon limitation is usually observed in high-latitude

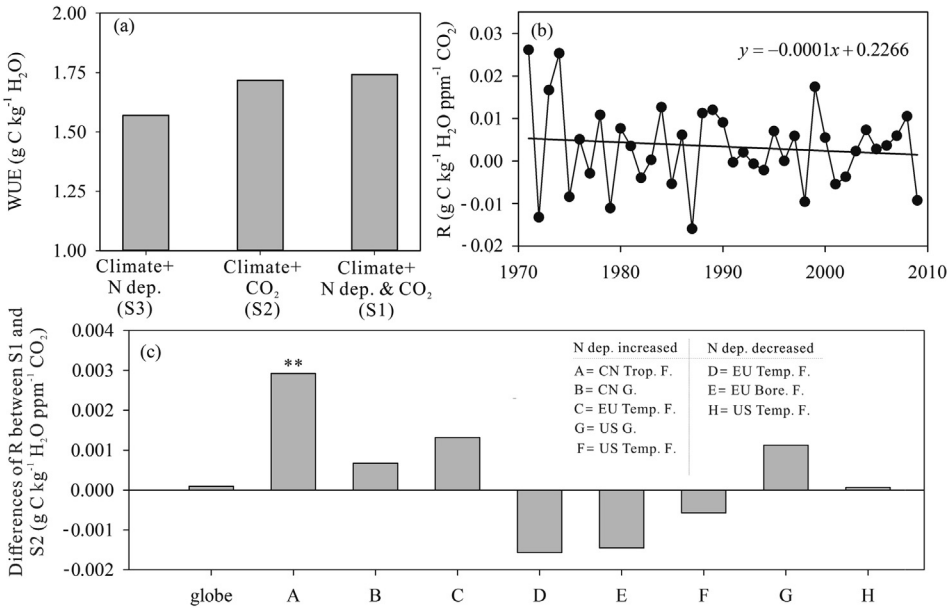

Fig. 6. Coupling effects of elevated CO_2 and increased N deposition on WUE. (a) Average WUE under different scenarios of simulation during 2000 to 2009. (b) Change in the response ratio (R) of WUE to elevated CO_2 from 1970 to 2009. (c) Differences in R between simulation S1 and S2 in 2000s on a global scale and at N deposition hotspots. ** Indicates statistical significance at the 99% ($P < 0.01$) level. CN, EU and US are represented China, Europe and United States, respectively. Trop, Temp and Bore are represented tropical, temperate and boreal, respectively. F and G are represented forest and grassland, respectively.

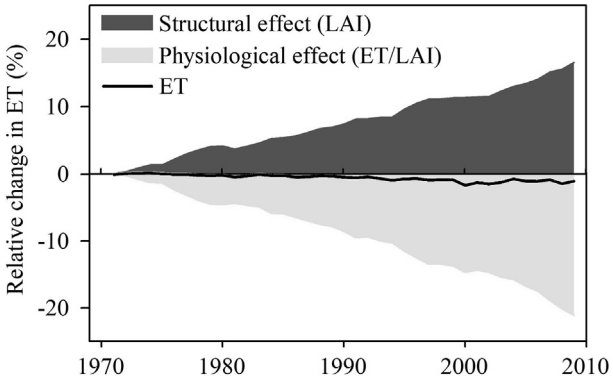

Fig. 7. Relative changes in ET in response to N deposition in southeastern China. The change of LAI and ET/LAI represent structural effects and physiological effects, respectively. The relative changes of LAI, ET/LAI and ET were extracted from a comparison between the scenarios of simulations S1 and S2.

regions (Handa et al., 2005), where carbon assimilation depends more on carbon availability in soil and not nitrogen availability (Koven et al., 2015). In tropical region, phosphorus availability limits primary productivity (Turner et al., 2018). Temperate forests are generally considered to be nitrogen-limited (Finzi et al., 2006), and in young subtropical and tropical forests, N addition can lead to significant increases in productivity (LeBauer and Treseder, 2008; Yu et al., 2016). Our results showed that the areas where WUE changed evidently by N deposition were mainly distributed in temperate and subtropical forests regions. Therefore, the increase in N deposition and the strong demand for N are the main reasons for the obvious impact of N on WUE in N deposition hotspots.

4.2. Changes in function and structure caused by nitrogen deposition

Our results showed that the ecosystem carbon and water cycles were changed by N deposition, and these changes were caused by changes of leaf physiology and ecosystem structure induced by N deposition. N addition increases leaf N concentration (Lu et al., 2011). According to the theory of Kull and Kruijt (1999), additional N in the leaf is allocated to 3 photosynthesis parameters: Rubisco, chlorophyll and electron transport rate. Therefore, increases in leaf N under N deposition enhances the leaf photosynthetic capacity. For the water cycle, stomatal conductance links transpiration and nutrient mass flow from the soil to leaf. The effectiveness of nutrient mass flow from the soil to leaf surface depends on transpiration and the nutrient state of the soil (Cramer et al., 2009). When the soil nutrient concentration is increased by N deposition, transpiration reduces to match the effectiveness of nutrient mass flow caused by a decrease in stomatal conductance (Cramer et al., 2009; Köhler et al., 2012; Livingston et al., 1999).

Ecosystem structural parameters, such as the LAI, are important when upscaling the impacts of N deposition from the leaf to canopy. N deposition increases both the LAI (Piao et al., 2015) and leaf photosynthetic capacity. Thus, the canopy photosynthetic capacity is enhanced by N deposition. In addition, nitrogen-induced enhancement of LAI leads to increases in canopy transpiration and canopy evaporation increase. However, soil evaporation is decreased under the greater amounts of shade induced by increased LAI. Accordingly, N deposition has a greater effect on GPP than ET.

Our results also showed a lower response of ET to high N deposition and found that N deposition had slightly negative effects on ET in southeastern China. To analyse the effects of N deposition on ET, we used ET/LAI and LAI to illustrate the physiological effects and structural effects, which were also employed by Huang et al. (2015) and Zhou et al. (2017) to analyse the effects of CO_2 on ET. As shown in Fig. 7, as N deposition increases, the relative change in the physiological effect (ET/LAI) was greater than that of the structural effect (LAI), which led to a decrease of ET in southeastern China.

Many models have simulated an increase in transpiration but a significant decrease in evaporation under increasing LAI (Zeng et al., 2018). Our model showed similar model behaviour, and the simulated ET declined by approximately 1% in southeastern China under high N deposition. However, due to the uncertainties of model parameterisations and the lack of observation-based constraints, current process-based models cannot accurately simulate T/ET well which results in pool performance of simulating ET responses to LAI change (Jasechko et al., 2013; Zeng et al., 2017). Nevertheless, our simulation shows that high N deposition in southeastern China led structural effect on ET enhanced more than other parts of the world.

4.3. Improved ability to simulate C-N coupling effects on WUE

Most models can simulate the promotion of WUE by elevated atmospheric CO_2 which is considered as a major factor in the change of WUE (Mao et al., 2015; Zhou et al., 2017). In addition, the effect of CO_2

on photosynthesis and stomata is also constrained by nitrogen. Therefore, the effects of CO_2 on WUE decline when N limitations are considered (Huang et al., 2015). According to our simulation, the response of WUE to elevated CO_2 (*R*) had been declined during the past 40 years which showed the progressing N limitation on WUE. However, N limitation was partially alleviated by increasing N deposition, which supplies more reactive N to the soil. In particular, the rapidly increasing N deposition in southeastern China has significantly increased the *R* of WUE under elevated CO_2, which is consistent with the finding that the comprehensive effects of CO_2 fertilization and N addition on WUE are greater than the individual effects of CO_2 (Köhler et al., 2012; Yan et al., 2014). Thus, the effect of N deposition on WUE cannot be ignored and need to be well evaluated under climate change.

Accurately simulating the effect of N deposition on the carbon-water coupling process is difficult (Zaehle et al., 2014) primarily because of a lack of long-term and valid observation data to constrain the model parameters. Our model is a C-N coupling model, and the ability to consider N limitation increases the consistency of our results with eddy flux tower observations (Fig. S1). However, the simulated results were still underestimated in the high value part (Fig. S1). The main error of the model may come from the empirical N constraint factor on important model parameters such as *V*max (Dickinson et al., 2002; Houborg et al., 2013). And inaccurate *V*max values introduce considerable errors into the simulation of photosynthesis and transpiration (He et al., 2017). Current research indicates that remotely sensed sunlight-induced chlorophyll fluorescence (Zhang et al., 2018) and chlorophyll (Croft et al., 2017) can accurately estimate *V*max at a large spatial scale. Therefore, the use of remote sensing data to optimize model parameters in the future will improve the simulation accuracy of the carbon-water coupling process.

5. Conclusions

In this study, the contribution of N deposition to global and regional changes in WUE was quantitatively characterized with the C-N coupling model IBIS-CN. N deposition, CO_2 and their coupling impacts were separated experimentally to determine the WUE variations between 1970 and 2009. The effects of N deposition on WUE has increased over the past 40 years. Enhanced N deposition promoted the WUE response to rising CO_2. N deposition also obviously impacted WUE in N deposition hotspot regions, where the ecosystem N demand is urgent. In these hotspots, the effect of N deposition on WUE was determined by GPP variations. The change in ET was offset by the increase in LAI caused by N deposition. Especially in southeastern China, the high N deposition reduced the response of ET to N deposition compared with that observed in other parts of the world. However, large uncertainties remain in the current IBIS-CN model in the effect of N on transpiration and root uptake. To accurately simulate and predict the response of WUE to N deposition, we suggest that the key parameters of photosynthesis and transpiration should be optimized using chlorophyll fluorescence and chlorophyll remote sensing data, which represent direct measurements at a large scale and over long time. Given the high probability that N deposition will continue to increase in the future, a better understanding and ability to predict the WUE response to N deposition would benefit local policy decisions to improve the strategies for water resource management and climate change mitigation.

Acknowledgments

Financial support for the study was provided by the National Key R &D Program of China (2016YFA0600202) and the National Natural Science Foundation of China (41871334, 41501212, 41471343). We acknowledge the support of the eddy covariance data provided by FLUXNET (http://fluxnet.fluxdata.org/).

Appendix A. Supplementary data

Supplementary data to this article can be found online at https://doi.org/10.1016/j.ecolind.2019.02.014.

References

Ball, J.T., Woodrow, I.E., Berry, J.A., 1987. A model predicting stomatal conductance and its contribution to the control of photosynthesis under different environmental conditions. Prog. Photosynthesis Res. 221–224. https://doi.org/10.1007/978-94-017-0519-6_48.

Beer, C., Ciais, P., Reichstein, M., Baldocchi, D., Law, B.E., Papale, D., Soussana, J.F., Ammann, C., Buchmann, N., Frank, D., Gianelle, D., Janssens, I.A., Knohl, A., Köstner, B., Moors, E., Roupsard, O., Verbeeck, H., Vesala, T., Williams, C.A., Wohlfahrt, G., 2009. Temporal and among-site variability of inherent water use efficiency at the ecosystem level. Glob. Biogeochem. Cycles 23, 1–13. https://doi.org/10.1029/2008GB003233.

Berry, J.A., Beerling, D.J., Franks, P.J., 2010. Stomata: key players in the earth system, past and present. Curr. Opin. Plant Biol. 13, 232–239. https://doi.org/10.1016/j.pbi.2010.04.013.

Cramer, M.D., Hawkins, H.J., Verboom, G.A., 2009. The importance of nutritional regulation of plant water flux. Oecologia 161, 15–24. https://doi.org/10.1007/s00442-009-1364-3.

Cramer, W., Bondeau, A., Woodward, F.I., Prentice, I.C., Betts, R.A., Brovkin, V., Cox, P.M., Fisher, V., Foley, J.A., Friend, A.D., Kucharik, C., Lomas, M.R., Ramankutty, N., Sitch, S., Smith, B., White, A., Young-Molling, C., 2001. Global response of terrestrial ecosystem structure and function to CO_2 and climate change: results from six dynamic global vegetation models. Glob. Chang. Biol. 7, 357–373. https://doi.org/10.1046/j.1365-2486.2001.00383.x.

Croft, H., Chen, J.M., Luo, X., Bartlett, P., Chen, B., Staebler, R.M., 2017. Leaf chlorophyll content as a proxy for leaf photosynthetic capacity. Glob. Chang. Biol. 23, 3513–3524. https://doi.org/10.1111/gcb.13599.

Dickinson, R.E., Berry, J.A., Bonan, G.B., Collatz, G.J., Field, C.B., Fung, I.Y., Goulden, M., Hoffmann, W.A., Jackson, R.B., Myneni, R., Sellers, P.J., Shaikh, M., 2002. Nitrogen controls on climate model evapotranspiration. J. Clim. 15, 278–295. https://doi.org/10.1175/1520-0442(2002) 015<0278:NCOCME>2.0.CO;2.

Du, E., Vries, W. De, 2018. Nitrogen-induced new net primary production and carbon sequestration in global forests. Environ. Pollut. 242, 1476–1487. https://doi.org/10.1016/j.envpol.2018.08.041.

Farquhar, G.D., von Caemmerer, S., Berry, J.A., 1980. A biochemical model of photosynthetic CO_2 assimilation in leaves of C_3 species. Planta 149, 78–90. https://doi.org/10.1007/BF00386231.

Fernández-Martínez, M., Vicca, S., Janssens, I.a., Sardans, J., Luyssaert, S., Campioli, M., Chapin III, F.S., Ciais, P., Malhi, Y., Obersteiner, M., Papale, D., Piao, S.L., Reichstein, M., Rodà, F., Peñuelas, J., 2014. Nutrient availability as the key regulator of global forest carbon balance. Nat. Clim. Chang. 4, 471–476. https://doi.org/10.1038/nclimate2177.

Finzi, A.C., Moore, D.J.P., DeLucia, E.H., Lichter, J., Hofmockel, K.S., Jackson, R.B., Kim, H.S., Matamala, R., McCarthy, H.R., Oren, R., Pippen, J.S., Schlesinger, W.H., 2006. Progressive nitrogen limitation of ecosystem processes under elevated CO_2 in a warm-temperate forest. Ecology 87, 15–25. https://doi.org/10.1890/04-1748.

Foley, J.A., Prentice, I.C., Ramankutty, N., Levis, S., Pollard, D., Sitch, S., Haxeltine, A., 1996. An integrated biosphere model of land surface processes, terrestrial carbon balance, and vegetation dynamics. Glob. Biogeochem. Cycles 10, 603–628. https://doi.org/10.1029/96gb02692.

Galloway, J.N., Dentener, F.J., Capone, D.G., Boyer, E.W., Howarth, R.W., Seitzinger, S.P., Asner, G.P., Cleveland, C.C., Green, P.A., Holland, E.A., 2004. Nitrogen cycles: past, present, and future. Biogeochemistry 70, 153–226.

Galloway, J.N., Townsend, A.R., Erisman, J.W., Bekunda, M., Cai, Z., Freney, J.R., Martinelli, L.a., Seitzinger, S.P., Sutton, M.a., 2008. Transformation of the nitrogen cycle: recent trends, questions, and potential solutions. Science 320, 889–892. https://doi.org/10.1126/science.1136.

Handa, I.T., Körner, C., Hättenschwiler, S., 2005. A test of the treeline carbon limitation hypothesis by in situ CO_2 enrichment and defoliation. Ecology. https://doi.org/10.1890/04-0711.

He, L., Chen, J.M., Croft, H., Gonsamo, A., Luo, X., Liu, J., Zheng, T., Liu, R., Liu, Y., 2017. Nitrogen availability dampens the positive impacts of CO_2 fertilization on terrestrial ecosystem carbon and water cycles. Geophys. Res. Lett. 44, 11590–11600. https://doi.org/10.1002/2017GL075981.

Houborg, R., Cescatti, A., Migliavacca, M., Kustas, W.P., 2013. Satellite retrievals of leaf chlorophyll and photosynthetic capacity for improved modeling of GPP. Agric. For. Meteorol. 117, 10–23. https://doi.org/10.1016/j.agrformet.2013.04.006.

Huang, M., Piao, S., Sun, Y., Ciais, P., Cheng, L., Mao, J., Poulter, B., Shi, X., Zeng, Z., Wang, Y., 2015. Change in terrestrial ecosystem water-use efficiency over the last three decades. Glob. Chang. Biol. 21, 2366–2378. https://doi.org/10.1111/gcb.12873.

Hungate, B.A., Reichstein, M., Dijkstra, P., Johnson, D., Hymus, G., Tenhunen, J.D., Hinkle, C.R., Drake, B.G., 2002. Evapotranspiration and soil water content in a scrub-oak woodland under carbon dioxide enrichment. Glob. Chang. Biol. 8, 289–298. https://doi.org/10.1046/j.1365-2486. 2002.00468.x.

Ito, A., Inatomi, M., 2012. Water-use efficiency of the terrestrial biosphere: a model analysis focusing on interactions between the global carbon and water cycles. J. Hydrometeorol. 13, 681–694. https://doi.org/10.1175/JHM-D-10-05034.1.

Jasechko, S., Sharp, Z.D., Gibson, J.J., Birks, S.J., Yi, Y., Fawcett, P.J., 2013. Terrestrial

water fluxes dominated by transpiration. Nature 496, 347–350. https://doi.org/10.1038/nature11983.
Keenan, T.F., Hollinger, D.Y., Bohrer, G., Dragoni, D., Munger, J.W., Schmid, H.P., 2013. Increase in forest water-use efficiency as atmospheric carbon dioxide concentrations rise. Nature 499, 324–327. https://doi.org/10.1017/CBO9781107415324.004.
Knauer, J., Zaehle, S., Reichstein, M., Medlyn, B.E., Forkel, M., Hagemann, S., Werner, C., 2017. The response of ecosystem water-use efficiency to rising atmospheric CO_2 concentrations: sensitivity and large-scale biogeochemical implications. New Phytol. 213, 1654–1666 doi: 10.11 11/nph.14288.
Köhler, I.H., MacDonald, A., Schnyder, H., 2012. Nutrient supply enhanced the increase in intrinsic water-use efficiency of a temperate seminatural grassland in the last century. Glob. Chang. Biol. 18, 3367–3376. https://doi.org/10.1111/j.1365-2486.2012.02781.x.
Koven, C.D., Lawrence, D.M., Riley, W.J., 2015. Permafrost carbon–climate feedback is sensitive to deep soil carbon decomposability but not deep soil nitrogen dynamics. Proc. Natl. Acad. Sci. https://doi.org/10.1073/pnas.1415123112.
Kucharik, C.J., Foley, J.A., Delire, C., Fisher, V.A., Coe, M.T., Lenters, J.D., Young-Molling, C., Ramankutty, N., Norman, J.M., Gower, S.T., 2000. Testing the performance of a dynamic global ecosystem model: water balance, carbon balance, and vegetation structure. Glob. Biogeochem. Cycles 14, 795–825. https://doi.org/10.1029/1999GB001138.
Kull, O., Kruijt, B., 1999. Acclimation of photosynthesis to light: a mechanistic approach. Funct. Ecol. 13, 24–36. https://doi.org/10.1046/j.1365-2435.1999.00292.x.
Lamarque, J.-F., Dentener, F., McConnell, J., Ro, C.U., Shaw, M., Vet, R., Bergmann, D., Cameron-Smith, P., Dalsoren, S., Doherty, R., Faluvegi, G., Ghan, S.J., Josse, B., Lee, Y.H., MacKenzie, I.A., Plummer, D., Shindell, D.T., Skeie, R.B., Stevenson, D.S., Strode, S., Zeng, G., Curran, M., Dahl-Jensen, D., Das, S., Fritzsche, D., Nolan, M., 2013. Multi-model mean nitrogen and sulfur deposition from the Atmospheric Chemistry and Climate Model Intercomparison Project (ACCMIP): evaluation of historical and projected future changes. Atmos. Chem. Phys. 13, 7997–8018. https://doi.org/10.5194/acp-13-7997-2013.
LeBauer, D.S., Treseder, K.K., 2008. Nitrogen limitation of net primary productivity in terrestrial ecosystems is globally distributed. Ecology 89, 371–379. https://doi.org/10.1890/06-2057.1.
Litton, C.M., Raich, J.W., Ryan, M.G., 2007. Carbon allocation in forest ecosystems. Glob. Chang. Biol. 13, 2089–2109. https://doi.org/10.1111/j.1365-2486.2007.01420.x.
Liu, J., Price, D.T., Chen, J.M., 2005. Nitrogen controls on ecosystem carbon sequestration: a model implementation and application to Saskatchewan, Canada. Ecol. Modell. 186, 178–195. https://doi.org/10.1016/j.ecolmodel.2005.01.036.
Liu, Y., Xiao, J., Ju, W., Zhou, Y., Wang, S., 2015. Water use efficiency of China's terrestrial ecosystems and responses to drought. Sci. Rep. 5, 13799. https://doi.org/10.1038/srep13799.
Livingston, N.J., Guy, R.D., Sun, Z.J., Ethier, G.J., 1999. The effects of nitrogen stress on the stable carbon isotope composition, productivity and water use efficiency of white spruce (Picea glauca (Moench) Voss) seedlings. Plant. Cell Environ. 22, 281–289. https://doi.org/10.1046/j.1365-3040.1999.00400.x.
Lu, M., Yang, Y., Luo, Y., Fang, C., Zhou, X., Chen, J., Yang, X., Li, B., 2011. Responses of ecosystem nitrogen cycle to nitrogen addition: a meta-analysis. New Phytol. 189, 1040–1050. https://doi.org/10.1111/j.1469-8137.2010.03563.x.
Lu, X., Jiang, H., Liu, J., Zhang, X., Jin, J., Zhu, Q., Zhang, Z., Peng, C., 2016a. Simulated effects of nitrogen saturation on the global carbon budget using the IBIS model. Sci. Rep. 6. https://doi.org/10.1038/srep39173.
Lu, X., Jiang, H., Zhang, X., Liu, J., Jin, J., 2016b. Estimating 40 years of nitrogen deposition in global biomes using the SCIAMACHY NO_2 column. Int. J. Remote Sens. 37, 4964–4978. https://doi.org/10.1080/01431161.2016.1225178.
Lu, X., Vitousek, P.M., Mao, Q., Gilliam, F.S., Luo, Y., Zhou, G., Zou, X., Bai, E., Scanlon, T.M., Hou, E., Mo, J., 2018. Plant acclimation to long-term high nitrogen deposition in an N-rich tropical forest. Proc. Natl. Acad. Sci. 115, 5187–5192. https://doi.org/10.1073/pnas.1720777115.
Mao, J., Fu, W., Shi, X., Ricciuto, D.M., Fisher, J.B., Dickinson, R.E., Wei, Y., Shem, W., Piao, S., Wang, K., Schwalm, C.R., Tian, H., Mu, M., Arain, A., Ciais, P., Cook, R., Dai, Y., Hayes, D., Hoffman, F.M., Huang, M., Huang, S., Huntzinger, D.N., Ito, A., Jain, A., King, A.W., Lei, H., Lu, C., Michalak, A.M., Parazoo, N., Peng, C., Peng, S., Poulter, B., Schaefer, K., Jafarov, E., Thornton, P.E., Wang, W., Zeng, N., Zeng, Z., Zhao, F., Zhu, Q., Zhu, Z., 2015. Disentangling climatic and anthropogenic controls on global terrestrial evapotranspiration trends. Environ. Res. Lett. 10, 94008. https://doi.org/10.1088/1748-9326/10/9/094008.
Niu, S., Classen, A.T., Dukes, J.S., Kardol, P., Liu, L., Luo, Y., Rustad, L., Sun, J., Tang, J., Templer, P.H., Thomas, R.Q., Tian, D., Vicca, S., Wang, Y.P., Xia, J., Zaehle, S., 2016. Global patterns and substrate-based mechanisms of the terrestrial nitrogen cycle. Ecol. Lett. 19, 697–709. https://doi.org/10.1111/ele.12591.
Piao, S., Yin, G., Tan, J., Cheng, L., Huang, M., Li, Y., Liu, R., Mao, J., Myneni, R.B., Peng, S., Poulter, B., Shi, X., Xiao, Z., Zeng, N., Zeng, Z., Wang, Y., 2015. Detection and attribution of vegetation greening trend in China over the last 30 years. Glob. Chang. Biol. 21, 1601–1609. https://doi.org/10.1111/gcb.12795.
Pinzon, J.E., Tucker, C.J., 2014. A non-stationary 1981–2012 AVHRR NDVI3g time series. Remote Sens. 6, 6929–6960. https://doi.org/10.3390/rs6086929.
Sun, Y., Piao, S., Huang, M., Ciais, P., Zeng, Z., Cheng, L., Li, X., Zhang, X., Mao, J., Peng, S., Poulter, B., Shi, X., Wang, X., Wang, Y.P., Zeng, H., 2016. Global patterns and climate drivers of water-use efficiency in terrestrial ecosystems deduced from satellite-based datasets and carbon cycle models. Glob. Ecol. Biogeogr. 25, 311–323. https://doi.org/10.1111/geb.12411.
Tang, X., Li, H., Desai, A.R., Nagy, Z., Luo, J., Kolb, T.E., Olioso, A., Xu, X., Yao, L., Kutsch, W., Pilegaard, K., Köstner, B., Ammann, C., 2014. How is water-use efficiency of terrestrial ecosystems distributed and changing on Earth? Sci. Rep. 4, 7483. https://doi.org/10.1038/srep07483.
Turner, B.L., Brenes-Arguedas, T., Condit, R., 2018. Pervasive phosphorus limitation of tree species but not communities in tropical forests. Nature 555, 367–370. https://doi.org/10.1038/nature25789.
Vet, R., Artz, R.S., Carou, S., Shaw, M., Ro, C.U., Aas, W., Baker, A., Bowersox, V.C., Dentener, F., Galy-Lacaux, C., Hou, A., Pienaar, J.J., Gillett, R., Forti, M.C., Gromov, S., Hara, H., Khodzher, T., Mahowald, N.M., Nickovic, S., Rao, P.S.P., Reid, N.W., 2014. A global assessment of precipitation chemistry and deposition of sulfur, nitrogen, sea salt, base cations, organic acids, acidity and pH, and phosphorus. Atmos. Environ. 93, 3–100. https://doi.org/10.1016/j.atm osenv.2013.10.060.
Wang, R., Goll, D., Balkanski, Y., Hauglustaine, D., Boucher, O., Ciais, P., Janssens, I., Penuelas, J., Guenet, B., Sardans, J., Bopp, L., Vuichard, N., Zhou, F., Li, B., Piao, S., Peng, S., Huang, Y., Tao, S., 2017. Global forest carbon uptake due to nitrogen and phosphorus deposition from 1850 to 2100. Glob. Chang. Biol. 23, 4854–4872. https://doi.org/10.1111/gcb.13766.
Yan, J., Zhang, D., Liu, J., Zhou, G., 2014. Interactions between CO_2 enhancement and N addition on net primary productivity and water-use efficiency in a mesocosm with multiple subtropical tree species. Glob. Chang. Biol. 20, 2230–2239. https://doi.org/10.1111/gcb.12501.
Yu, G., Chen, Z., Piao, S., Peng, C., Ciais, P., Wang, Q., Li, X., Zhu, X., 2014. High carbon dioxide uptake by subtropical forest ecosystems in the East Asian monsoon region. Proc. Natl. Acad. Sci. https://doi.org/10.1073/pnas.1317065111.
Yu, G., Ren, W., Chen, Z., Zhang, L.L., Wang, Q., Wen, X., He, N., Zhang, L.L., Fang, H., Zhu, X., Gao, Y., Sun, X., 2016. Construction and progress of Chinese terrestrial ecosystem carbon, nitrogen and water fluxes coordinated observation. J. Geogr. Sci. 26, 803–826. https://doi.org/10.1007/s11442-016-1300-5.
Zaehle, S., Medlyn, B.E., De Kauwe, M.G., Walker, A.P., Dietze, M.C., Hickler, T., Luo, Y., Wang, Y.P., El-Masri, B., Thornton, P., Jain, A., Wang, S., Warlind, D., Weng, E., Parton, W., Iversen, C.M., Gallet-Budynek, A., Mccarthy, H., Finzi, A., Hanson, P.J., Prentice, I.C., Oren, R., Norby, R.J., 2014. Evaluation of 11 terrestrial carbon-nitrogen cycle models against observations from two temperate free-air CO_2 enrichment studies. New Phytol. 202, 803–822. https://doi.org/10.1111/nph.12697.
Zeng, Z., Peng, L., Piao, S., 2018. Response of terrestrial evapotranspiration to Earth's greening. Curr. Opin. Environ. Sustain. 33, 9–25. https://doi.org/10.1016/j.cosust.2018.03.001.
Zeng, Z., Piao, S., Li, L.Z.X., Zhou, L., Ciais, P., Wang, T., Li, Y., Lian, X., Wood, E.F., Friedlingstein, P., Mao, J., Estes, L.D., Myneni, R.B., Peng, S., Shi, X., Seneviratne, S.I., Wang, Y., 2017. Climate mitigation from vegetation biophysical feedbacks during the past three decades. Nat. Clim. Chang. 7, 432–436. https://doi.org/10.1038/nclimate3299.
Zhang, Y., Guanter, L., Joiner, J., Song, L., Guan, K., 2018. Spatially-explicit monitoring of crop photosynthetic capacity through the use of space-based chlorophyll fluorescence data. Remote Sens. Environ. 210, 362–374. https://doi.org/10.1016/j.rse.2018.03.031.
Zhang, Z., Jiang, H., Liu, J., Ju, W., Zhang, X., 2013. Effect of heterogeneous atmospheric CO_2 on simulated global carbon budget. Glob. Planet. Change 101, 33–51. https://doi.org/10.1016/j.gloplacha.2012.12.002.
Zhou, S., Yu, B., Schwalm, C.R., Ciais, P., Zhang, Y., Fisher, J.B., Michalak, A.M., Wang, W., Poulter, B., Huntzinger, D.N., Niu, S., Mao, J., Jain, A., Ricciuto, D.M., Shi, X., Ito, A., Wei, Y., Huang, Y., Wang, G., 2017. Response of water use efficiency to global environmental change based on output from terrestrial biosphere models. Glob. Biogeochem. Cycles 31, 1639–1655. https://doi.org/10.1002/2017GB005733.
Zhu, Q.A., Jiang, H., Peng, C., Liu, J., Fang, X., Wei, X., Liu, S., Zhou, G., 2012. Effects of future climate change, CO_2 enrichment, and vegetation structure variation on hydrological processes in China. Glob. Planet. Change 80–81, 123–135. https://doi.org/10.1016/j.gloplacha.2011.10.010.
Zhu, Q.A., Jiang, H., Peng, C.H., Liu, J.X., Wei, X.H., Fang, X.Q., Liu, S.R., Zhou, G.M., Yu, S.Q., 2011. Evaluating the effects of future climate change and elevated CO_2 on the water use efficiency in terrestrial ecosystems of China. Ecol. Modell. 222, 2414–2429. https://doi.org/10.1016/j.ecolmodel.2010.09.035.
Zhu, Z., Piao, S., Myneni, R.B., Huang, M., Zeng, Z., Canadell, J.G., Ciais, P., Sitch, S., Friedlingstein, P., Arneth, A., Cao, C., Cheng, L., Kato, E., Koven, C., Li, Y., Lian, X., Liu, Y., Liu, R., Mao, J., Pan, Y., Peng, S., Peñuelas, J., Poulter, B., Pugh, T.A.M., Stocker, B.D., Viovy, N., Wang, X., Wang, Y., Xiao, Z., Yang, H., Zaehle, S., Zeng, N., 2016. Greening of the Earth and its drivers. Nat. Clim. Chang. 6, 791–795. https://doi.org/10.1038/nclimate3004.